Journal of Applied Research and Technology

www.jart.icat.unam.mx

Journal of Applied Research and Technology 23 (2025) 310-321

Original

Adaptive Archimedes optimization algorithm trained deep learning for polycystic ovary syndrome detection using ultrasound image

K. R. Shelke

Department of Computer Engineering, Agnel Charities, Fr. C. Rodrigues Institute of Technology, Vashi, Navi Mumbai, India

Received 08 13 2024; accepted 12 11 2024
Available 08 31 2025

Abstract: Polycystic ovary syndrome (PCOS) disorder is caused by a protracted menstruation cycle that frequently elevated the androgen levels of women in their reproductive age. Insulin resistance affects 50% to 70% of all women with PCOS, and hormone difference contributes to the high levels of testosterone that causes the symptoms and signs of PCOS. This work develops a deep learning (DL) based PCOS diagnosis to address these issues. At the initial stage, the ultrasound image is preprocessed utilizing an adaptive Wiener filter for the noise removal process. The Polycystic ovary (PCO) follicles segmentation process is performed using the Fuzz Local C-Means Clustering (FLICM). Feature extraction is the next stage, where the Speeded-Up Robust Feature (SURF), Shape index histogram as well as the statistical features includes variance, mean, kurtosis, entropy, and standard deviation are extracted. Furthermore, the PCOS detection is done in the next stage, where a deep Q Net (DQN) is utilized and the parameters of DQN are optimized by the adaptive Archimedes optimization algorithm (AOA). Moreover, the system performance is evaluated using accuracy, sensitivity, and specificity parameters with corresponding values like 0.906, 0.918, and 0.928.

Keywords: Polycystic ovary syndrome, deep learning, Archimedes optimization algorithm, deep Q Net, ultrasound image.

*Corresponding author.
E-mail address: Kavita.shelke@fcrit.ac.in (K. R. Shelke).
Peer Review under the responsibility of Universidad Nacional Autónoma de México.

1. Introduction

Polycystic ovary syndrome (PCOS) is a health issue (Wisesty et al., 2018) that causes hormonal imbalances in women throughout their reproductive stage (Nasim et al., 2022). The hormone imbalance causes the ovaries that produce a small volume of fluid known as follicles (cysts). Due to PCOS, the ovaries fail to produce eggs, which is a common problem in women and causes serious pregnancy complications (Suha & Islam, 2022). PCOS is a hormonal disorder that causes fertility issues (Alamoudi et al., 2023). PCOS disease is typically inherited and is a life-threatening emergency. Rising acne, increased body and facial hair, alopecia, obesity, infertility, and irregular periods are the signs and symptoms of PCOS (Wisesty et al., 2017). Ultrasound imaging is one method for gathering images from human organs using sound waves of higher frequency. The echoes from the reflected sound waves are registered and presented as a concurrent visual image. The internal organs of the body such as the heart, liver, gallbladder, kidneys, and ovaries, can be examined by this technique. The detection of follicles in ovaries through ultrasound images involved the follicle controlling during the clinical diagnosis of a patient's infertility treatment (Nilofer & Ramkumar, 2021). Ultrasound has several merits compared to other medical imaging procedures like magnetic resonance imaging (MRI) and computed tomography (CT). Moreover, the ultrasound is inexpensive, easily accessible, and offers real-time results (Gopalakrishnan & Iyapparaja, 2020).

Morphological operators frequently take a binary image accompanied by closing and opening the operations to extract the bright features from the background of ultrasound images (Deng et al., 2011). The typical computational approaches to detecting PCOS rely on many techniques such as image processing, feature extraction, and then conventional Machine learning (ML) techniques for image classification, which is a time-consuming process with relatively low performance (Suha & Islam, 2022). The ML analyses the data and converts it into a usable format for clinical procedures, and it aids in determining the nature of various diseases (Nasim et al., 2022). Many ML and DL methods including Support Vector Machine (SVM) (Gopalakrishnan & Iyapparaja, 2019), Naive Bayes (NB), Convolution Neural Network (CNN) (McLaughlin et al., 2017), and Visual Geometry Group (VGG-16) (Shabani et al., 2020) have been applied to produce ovary ultrasound image analyses for diagnosis systems. In the medical field, three types of ML methods are used. The relevant features were adapted for training a Probabilistic Neural Network (PNN) to differentiate the affected and nonaffected images. The Artificial Neural Network (ANN) is crucial in classifying carcinogenic ovarian conditions. The ovarian follicle image was automatically segmented using the k-means clustering technique (Nasim et al., 2022). Consequently, the DL approach is used to make the training process in simple manner and it attain better results because DL does not require a manual process of feature extraction. During model training, the CNN can automatically extract features (Gopalakrishnan & Iyapparaja, 2020).

The important goal of this work is to offer an effectual detection of PCOS using adaptive AOA enabled DQN. This approach employed an adaptive wiener filter-based image preprocessing and FLICM based segmentation process. Afterwards, the crucial features are extracted and the PCOS detection is achieved with the help of adaptive AOA trained DQN.

The foremost contribution of this work is deliberated as follows.

- Proposed adaptive AOA-DQN for PCOS detection: The PCOS disease is identified using DQN, which is trained with the help of the proposed adaptive AOA. Here, the adaptive AOA increases the effectiveness of PCOS disease detection.

The remaining section of this paper is arranged as follows: Section 2 comprises a review of the literature on traditional methods of PCOS detection, as well as their merits and drawbacks. Section 3 deliberates the proposed methods. Section 4 describes the result of the proposed system. Section 5 clarifies the conclusion section.

2. Motivation

PCOS is a hormonal syndrome of females in reproductive ages. Hence, PCOS diagnosis is essential for early-stage treatment. Various existing methodologies were utilized in PCOS detection process. Still, they take more computation time. For reducing the processing time and providing simple implementation, the adaptive AOA enabled DQN is utilized here.

2.1. Literature survey

Wisesty et al. (2018) developed the Global Basic Threshold and Otsu Threshold method based PCOS detection process. Here, the image binarization and follicle segmentation calculate the number and diameter of the follicle. The algorithm was effective for minimizing the time and space requirements. But the output contained a small amount of noise. Suha and Islam (2022) developed the ML classification technique for PCOS prediction. Here, CNN was integrated with different state-of-the-art techniques. This technique was successful in achieving the best performances in the least execution time and can be applied to real-world scenarios. Still, this technique resulted in high computational complexity. Nilofer and Ramkumar, (2021) devised an improved Fruit Fly Optimization (IFFOA) for PCOS prediction. The adaptive k-means clustering was applied for processing the follicle segments. This technique was quite robust to reduce the noise of training data. Still, it failed to process the alternative medical data. Kiruthika et al. (2020)

developed the ML based ovarian detection (MLOD) for detecting PCOS. Here, the detection and ovarian classification were based on the combination of texture features and intensity and provided the classification in a fast manner. Still, it did not segment the intermolecular regions. Table 1 shows the summary of the methods, advantages, and limitations of the reviewed studies. Sarty et al. (1998), introduced a method for automatically detecting the outer boundaries of follicle walls in ultrasound images of the ovary. The approach utilizes prior knowledge about edge direction and intensity, as well as the characteristics of follicle walls and typical follicle shapes, to analyze ovary images. The technique involves segmenting the follicle of interest as identified by the physician, followed by the calculation of features such as follicle size, root mean square deviations of fluid signals, and wavelet packet energy to aid in disease detection. Viher et al. (1998) utilized Cellular Automata to identify follicles in ultrasound images of the ovary, dividing the process into two stages. In the first stage, each object in the image developed an "immune system" to characterize its boundary cell features. In the second stage, a large-scale "attack" was launched against these immune systems, effectively eliminating phantom follicles while preserving real ones. However, the method was limited by its high computational complexity. Lawrence et al. (2007) proposed a novel method to distinguish between normal and polycystic ovaries. They utilized a region-growing algorithm for segmentation, followed by the extraction of features such as volume density, surface density, the number of follicle regions per image, maximum follicle diameter, and mean follicle diameter, which were combined into a feature vector. For classification, they applied k-nearest neighbor, linear discriminant, and SVM methods, reporting that the linear discriminant approach achieved the highest classification accuracy. Hiremath and Tegnoor (2010a) utilized Gaussian low-pass filters and contourlet transforms to reduce speckle noise in ultrasound ovary images. They employed the Canny edge detector for segmentation and calculated the lengths of the major and minor axes, using these features to develop classification rules for distinguishing follicles from non-follicles. The study reported a follicle detection rate of 75.2% with the contourlet transform, compared to 62.3% using the Gaussian low-pass filter. Hiremath and Tegnoor (2010b), proposed the preprocessing phase using a Wiener filter to reduce speckle noise, followed by negative transformation, histogram equalization, and morphological operations to obtain a denoised image. The active contour without edge method is then applied for segmentation. From the segmented image, texture features such as contrast, correlation, energy, and homogeneity are extracted using the grey-level co-occurrence matrix. These texture features are then classified into follicles and non-follicles using a multi-layer perceptron neural network.

Table 1. Summary of PCOS detection techniques

Reference	Method Used	Advantages	Limitations
Wisesty et al. (2018)	Global Basic Threshold and Otsu Threshold for PCOS detection	Minimizes time and space requirements	Output contains some noise
Suha and Islam (2022)	CNN integrated with state-of-the-art techniques	High performance in minimal execution time, practical	High computational complexity
Nilofer and Ramkumar (2021)	Improved Fruit Fly Optimization Algorithm (IFFOA) with adaptive k-means clustering	Robust to reduce training data noise	Fails to process alternative medical data
Kiruthika et al. (2020)	Combination of texture features and intensity	Fast Classification	Do not accurately segment the intermolecular regions.
Sarty et al. (1998)	Edge-based segmentation approach	Automates boundary detection with improved accuracy, extracts clinically relevant features, and aligns with physician priorities.	It depends on predefined knowledge, is sensitive to image quality, requires physician input, and has limited adaptability to other imaging contexts
Viher et al. (1998)	Two-stage Cellular Automata approach	Effectively differentiates real follicles from phantom	Suffers from high computational complexity
Lawrence et al. (2007)	Region-growing segmentation, extracted follicle features for a feature vector, and classified using k-NN,	Accurate differentiation between normal and polycystic ovaries with effective feature extraction and classification	Performance depends on the quality of segmentation and the choice of features and classifiers
Hiremath and Tegnoor (2010a)	Gaussian low-pass filters and contourlet transforms for noise removal, Canny edge detection for segmentation,	Achieves higher detection accuracy with contourlet transforms compared to	Moderate detection rates indicate room for improvement in classification accuracy.

	and axis-based features to classify follicles	Gaussian filtering.	
Hiremath and Tegnoor (2010b)	Wiener filter reduces speckle noise, followed by preprocessing and active contour segmentation, with texture features classified using a multi-layer perceptron neural network.	Effectively reduces noise and classifies follicles with texture features.	Relies on multiple preprocessing steps, which may increase computational complexity.

2.2. Challenges

Challenges that occurred in PCOS detection process are detailed below:

- In Wisesty et al. (2018), the CNN model helps the physician to save the time requirement for assessing the patients and decrease the risk level of delayed diagnosis. However, the lack of available computational resources affected the system's performance.
- Thresholding method based PCOS detection (Suha & Islam, 2022) technique performed effectively in the real-world application. However, this work was futile in reducing the computational complexity.
- In Kiruthika et al. (2020), MLOD classifier failed to avoid the uncertainty of cystic ovary classification by including demographic data that includes the texture and intensity features.
- PCOS is the most common female endocrine disorder. Hence, numerous PCOS detection techniques have been employed. Still, the signs of PCOS differ with weight, medications, and age. Hence, the accurate diagnosis of PCOS is highly critical.

3. Proposed adaptive AOA – DQN for PCOS detection

The prime goal of this work is to develop an Adaptive AOA trained deep learning for PCOS detection using ultrasound images. Initially, the input ultrasound is converted into gray form. Afterward, it is fed to the preprocessing, where an Adaptive wiener filter (Wu et al., 2020) is adopted to remove noises. Then, the preprocessed image is fed to PCOS follicles segmentation module, where the FLICM (Krinidis & Chatzis, 2010) is employed to segment the PCOS. Afterward, feature extraction is performed to reduce the number of resources required to describe a large set of images, wherein features, such as Speeded-Up Robust Features (SURF) (Bay et al., 2008), Shape Index Histograms (Larsen et al., 2014), and statical features (Khairandish et al., 2022) like, mean, variance, kurtosis, standard deviation, and entropy are extracted. Subsequently, PCOS detection is done by DQN (Sasaki et al., 2017), which is trained by the proposed Adaptive AOA, and it is designed by the integration of AOA (Hashim et al., 2021) with the adaptive concept Figure 1. Shows the block diagram of Adaptive AOA-DQN for PCOS detection using ultrasound image.

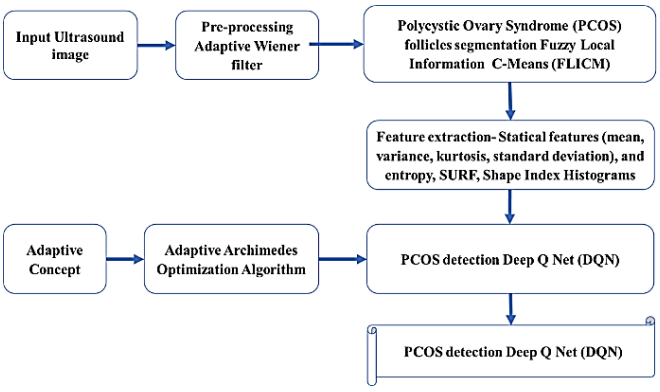

Figure 1. Block diagram of the adaptive AOA_DQN for PCOS detection using ultrasound image.

3.1. Image Acquisition

The ultrasound images are taken from a dataset, which is denoted as,

$$E = \{E_1, E_2 \ldots\ldots E_j, \ldots, E_t\} \quad (1)$$

Here, E indicates the ultrasound image database, t symbolizes the total images contained by the dataset E .The j^{th} image E_j is utilized for further procedures.

3.2. Image pre-processing

Pre-processing is used for neglecting the noise contents from the input image after gray conversion. The image E_j is forwarded as the input of pre-processing. Here, the preprocessing stage utilized an adaptive Wiener filtering.

3.2.1. Adaptive Wiener filter

Adaptive wiener filtering (Wu et al., 2020) adjusts the filter's output with respect to the local variation of image pixels. The minimization of mean square error (MSE) between the recovered as well as original image is considered as the initial stage of this filtering scheme. The image filtering has been contaminated by the signal-to-noise. It can be demonstrated as,

$$n(s,t) = o(s,t) + q(s,t) \quad (2)$$

where $n(s,t)$ implies the noisy part of the image, $o(s,t)$ shows the noiseless image, $q(s,t)$ implies an additive noise.

Here, the noise $n(s,t)$ is eliminated and the filtered output image is represented as E_n.

3.3. Adaptive Wiener filter

In PCO follicle segmentation, the FLICM (Krinidis & Chatzis, 2010) uses the neighborhood information of each image pixel in order to achieve image clustering. Here, a pre-processed image E_n is given as the input for segmentation. It provides a grey level and spatial information for attaining a wide range of features. The neighboring samples for every vector α_μ is computed, where a fuzzy factor is given as, $D_{\Re\mu}$.

$$D_{\Re\mu} = \sum_{\substack{\rho\epsilon \square_\mu \\ \mu\neq\rho}} \frac{1}{\sigma_{\mu,\rho}+1}(1-c_{\Re\rho})^\beta \, I(\alpha_\rho, d_\Re)^2 \quad (3)$$

where, μ^{th} denotes the data vector under vector representation, $\Re$ indicates the reference cluster and the ρ^{th} represents the neighboring data vector in a set μ^{th} of data vector $(\square_\mu)$. $\sigma_{\mu,\rho}$ indicates a spatial Euclidean distance among the data vectors μ^{th} and ρ^{th} in $\square$ dimension space. Moreover, $I(.)$ specifies the distance function that measures the resemblance among two data vectors. Here, the weighting exponent on every fuzzy membership is indicated as β, and $d_\Re$ specifies the model of centre cluster $\Re$. Furthermore, the segmented output image E_0 is gathered from the FLICM.

3.4. Feature extraction

Feature extraction is utilized to minimize the redundant data. Moreover, the features include SURF, Shape index histogram and statistical features and are extracted. Here, the PCO follicles segmented image E_0 is forwarded as the input of feature extraction and the output feature vector is obtained using the following processes.

a) *Shape index Histogram*: The shape index (Larsen et al., 2014) is an image geometry that captures the second-order image structure in a continuous interval which allows to summarize the distribution of curvatures in a histogram. Here, a shape index is gathered from Hessian matrix $\Delta^2 K$, in which a second-order curvature of scale is captured. Moreover, the shape index is given as,

$$\Delta^2 K(\lambda,n) = \begin{bmatrix} K_{\lambda^2} & K_{\lambda\chi} \\ K_{\lambda\chi} & K_{\chi^2} \end{bmatrix} \quad (4)$$

where, $\Delta^2 K$ indicates the Hessian matrix along with λ, χ, and direction. η specifies the second-order curvature. The output image after shape index histogram is indicated as E_{p1}, *b) SURF*: SURF (Bay et al., 2008) is employed to extract the local robust feature using a Hessian matrix-based measure. Here, the interest area is separated as $4X4$ sub areas that are defined by a wavelet response in a and b directions that it is represented as da and db. In each sub area, the vector H is estimated by a $5X5$ samples.

$$H = \{\sum da, \sum|da|, \sum db, \sum|db|\} \quad (5)$$

Here, the output image comes from the SURF is specified as E_{p2}. The output image after Shape index Histogram and SURF is represented as E_p, which is represented as,

$$E_p = \{E_{p1}, E_{p2}\} \quad (6)$$

c) *Statistical Features:* In statistical feature extraction (Polycystic Ovary Ultrasound Images Dataset, 2023), the image E_p is given as the input. Here, the features include variance, mean, kurtosis, entropy and standard deviation are extracted.

Variance: Average value of squared difference among every sample and its mean value is known as variance and it is represented as g_1.

Mean: The proportion of pixel intensity to the whole number of pixels is termed as mean. It is specified as g_2.

Kurtosis: Relative flatness of peakness while it is compared to a regular allocation is named as Kurtosis. Here g_3 denotes the kurtosis parameter.

Entropy: Entropy is utilized for estimating the diversity of images and it is employed to indicate the quality image. Here, the entropy is indicated as g_4.

Standard Deviation: It is a crucial factor for defining the difference between the mean value. Moreover, it is defined as the general square of variance and it is denoted as g_5.

The statistical features are denoted in vector representation,

$$G = \{g_1, g_2, g_3, g_4\} \quad (7)$$

3.5. PCOS detection using deep Q-network

The PCOS detection is performed with the help of DQN (Polycystic Ovary Ultrasound Images Dataset, 2023). It employs the Q-learning process which provides superior reinforcement learning that uses the CNN for detecting the approximate action value function called as Q-function. Here, figure 2 represents the structure of DQN. It contains a fully connected, max pooling as wells convolutional layers. Here, the neural network (NN) is employed for representing the action-value function (W-function). Here the image G is considered as the input of DQN. Max pooling is commonly utilized in Convolutional Neural Networks (CNNs) for downsampling, as it selects the maximum value from a set of features, retaining the most significant information. This helps in reducing the spatial dimensions of the data while maintaining important features.

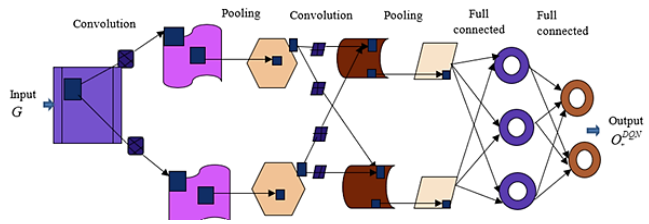

Figure 2. Architecture of Deep Q-network.

The Q-learning updates a sample of experience (i_e, u_e, m_e, i_{e+1}) drawn regularly from a data set. The following loss function are updated by the Q-learning,

$$F_\Psi(\theta_\Psi) = V\left[\left(m + \zeta \max_{u'} \dot{X}(\iota', \dot{u}'; \theta_{\bar{\Psi}}) - X(e, i; \theta_\Psi)\right)^2\right] \quad (8)$$

where, m indicates a reward, ς signifies the discount factor, a network constraints of Q-network in Ψ^{th} iteration is denoted as θ_Ψ is a and $\theta_{\bar{\Psi}}$ implies the network parameters. For improving the convergence stability, DQN utilized the neural fitted Q method, where the parameter θ in the target $m + \zeta \max_{u'} X(\iota', \dot{u}'; \theta_\Psi)$ is represented as $m + \zeta \max_{u'} X(\iota', \dot{u}'; \theta_{\bar{\Psi}})$ at the certain period. Here, the detected output image is indicated as Q_r^{DQN}.

3.5.1. Adaptive AOA based training of DQN

The AOA (Sasaki et al., 2017) is a kind of population-based algorithm, in which the individuals in the population are serves as an immersed object. AOA begins the search method using the initial population of candidate solutions. It possesses the similar accelerations, densities and random volumes with respect to other population-based metaheuristic algorithms. In every iteration, the volume as well as density of every item is updated by AOA. The AOA providing few parameters that offers simple implementation. Moreover, the adaptive concept is added to AOA for reducing the computation time. The mathematical description of adaptive AOA stages is expressed below.

Step 1. Initialization: Initiate the object's position using the following equation

$$A_h = L_{s_h} + rand * \left(U_{S_h} - L_{S_h}\right), h = 1,2, \ldots, [] \quad (9)$$

where A_h represents the h^{th} object at the population of [] objects. The upper and lower bounds of a search position is indicated as U_{S_h}, L_{S_h}. The density, $(\Im)$ volume of h^{th} object is given as,

$$\lambda_h = rand \quad (10)$$

$$\Im_h = rand \quad (11)$$

where $rand$ indicated the vector, which are generated randomly between $(0,1)$ values. Moreover, the initial acceleration in h^{th} object is given as,

$$\wp_h = L_{S_h} + rand * \left(U_{S_h} - L_{S_h}\right) \quad (12)$$

Here, the initial population and the selected objects are estimated with the finest value.

Step 2. Fitness function estimation: The finest solution is predicted with respect to the fitness value. The fitness with low value of MSE is deliberated the best solution. The fitness of adaptive AOA is,

$$Fittness = \frac{1}{t}\sum\left(O_r^* - O_r^{DQN}\right)^2 \quad (13)$$

where, the entire images gathered from the dataset id indicated as t. The output of DQN is denoted as Q_r^{DQN} and the targeted output is stated as Q_r^*.

Step 3. Update the density (λ) and volume $(\Im)$: The density as well as volume of h^{th} object in $(f+1)$ iteration is updated as,

$$\lambda_h^{f+1} = \lambda_h^f + rand * \left(\lambda_{best} - \lambda_h^f\right) \quad (14)$$

$$\Im_h^{f+1} = \Im_h^f + rand * \left(\Im_{best} - \Im_h^f\right) \quad (15)$$

where, λ_h^f indicates the density of f iteration λ_h^{f+1}, represents the density at $f+1$ iteration, the volume at f and $f+1$ iteration are indicated as $\Im_h^f$ and $\Im_h^{f+1}$, the density and volume of the best solution is defined as λ_{best} and $\Im_{best}$.

Step 4. Estimation of density factor and transfer operator: At the initial stage, the collision occurs in between the objects. After a certain period, the objects can achieve the equilibrium position using the transfer operator,

$$T_f = Exp\left(\frac{w - w_{max}}{w_{max}}\right) \quad (16)$$

where transfer T_f growths gradually with time until reaching to 1. Here w indicates the iteration number and W_{max} signifies the maximum iteration counting. Likewise, the density diminishing factor q supports the AOA on global to local search and it is given as,

$$q^{f+1} = Exp\left(\frac{f_{max} - 1}{f_{max}}\right) - \left(\frac{f}{f_{max}}\right) \quad (17)$$

where $(f+1)$ is reduced with time of converge in the identified promising region. The maximum iteration and the iteration number is specified as f_{max} and f.

Step 5 a). Exploration phase (Collision between the objects occurred): In this case, $if\ T_f \leq 0.5$, a collision occurred between the objects, then a random material ξ. The acceleration in an object is updated as,

$$\wp_h^{f+1} = \frac{\lambda_\xi + \Im_\xi * \wp_\xi}{\lambda_h^{f+1} * \Im_h^{f+1}} \quad (18)$$

where, the volume $\Im_\xi$, acceleration $\wp_\xi$ and density λ_ξ are the crucial part of acceleration.

Step 5 b). Exploitation phase (Objects with no collision): In this phase $if\ T_f > 0.5$ there are no collision. The acceleration of updated object at iteration is given as,

$$\Im_h^{f+1} = \frac{\lambda_{best} + \Im_{best} * \wp_{best}}{\lambda_h^{f+1} * \Im_h^{f+1}} \quad (19)$$

where, the best object's acceleration is expressed as $\wp_{best}$.

Step 5 c). Normalize acceleration: The Normalize acceleration is employed to compute the percentage of variation. It is given by,

$$\wp_{h-norm}^{f+1} = x * \frac{\wp_h^{f+1} - \min(\wp)}{\max(\wp) - \min(\wp)} + y \quad (20)$$

where x and y represents the normalization range, which are set as 0.9 and 0.1. Here, $\wp_{h-norm}^{f+1}$ regulates the percentage change, while each agent will change.

Step 6. Position update: In this phase, $if\ T_f \leq 0.5$ the position of h^{th} object in next iteration $(f+1)$ using the following equation,

$$\lambda_h^{f+1} = \lambda_h^f + J_1 * rand * \wp_{h-norm}^{f+1} * q * \left(\lambda_{rand} - \lambda_f^f\right) \quad (21)$$

where, the value of constant J_1 is set as 2.The parameter $rand$ is considered as adaptive.

$$rand = \left(1 - \frac{f}{Iter_{max}}\right) * \frac{(2 * rand(0.05))}{J_2} \quad (22)$$

where, J_2 represents the constant, which is equal to 0.6. the current iteration is specified as f and the maximum iteration is deliberated as $Iter_{Max}$,

Step 7. Re-evaluation of fitness: Fitness of updated solution is valued, and a solution providing lesser fitness is taken as the desirable solution.

Step 8. Termination: The optimal weights are generated till the extreme level of iterations are accomplished. The adaptive AOA algorithm's pseudocode is defined in table 1.

4. Results and discussion

This work provides the detection of PCOS using adaptive AOA-DQN, in which the performance of AOA-DQN is investigated using the dataset, performance metrics. Moreover, the assessment of adaptive AOA-DQN based PCOS detection is described here. The adaptive AOA-DQN for PCOS detection is implemented in MATLAB.

4.1. Dataset description

The Polycystic Ovary Ultrasound Images Dataset (Polycystic Ovary Ultrasound Images Dataset, 2023) covers the ultrasound images of normal patients and the patients suffering from PCOS. The Polycystic Ovary Ultrasound Images Dataset, hosted on the Telkom University Dataverse, consists of ultrasound images used to analyze polycystic ovary syndrome (PCOS). Key characteristics include:

- Content: The dataset includes images representing both normal and polycystic ovary conditions, categorized appropriately. This enables its use in training diagnostic systems.
- File Types: The images are in JPEG format, with sizes typically under 30 KB, ensuring they are lightweight for computational use.
- Annotation: The dataset is structured with clearly labeled categories to support supervised machine learning tasks, such as classification or detection models.

From this dataset 74% images are of normal patients and 26% are the images of patients suffering from PCOS. The 60% images are used for training, 40%are used for testing.

4.2. Performance metrics

The performance metrics utilized for PCOS detection contains accuracy, specificity, and sensitivity.

4.2.1. Accuracy

Accuracy is termed as a total quantity of sameness among the raw value and the projected rate. It is specified as,

$$Accuracy = \frac{B(+) + B(-)}{B(+) + B(-) + C(+) + C(-)} \quad (23)$$

4.2.2. Sensitivity

Sensitivity indicates overall count of positives obtained by the detection. It is described as,

$$Sensitivity = \frac{B(+)}{B(+) + C(-)} \quad (24)$$

4.2.3. Specificity

The overall quantity of negatives obtained by the detection is stated as specificity. It is given as,

$$Specificity = \frac{B(-)}{B(-)+C(+)} \quad (25)$$

4.3. Experimental outcomes

The image scrutiny of adaptive AOA-DQN for PCOS detection is portrayed in figure 3. Ere, an input images is shown in figure 3a), and the related gray, filtered, FLIC, SURF, Shape index histogram images are shown in figures 3 b), c), d), e) and f) respectively.

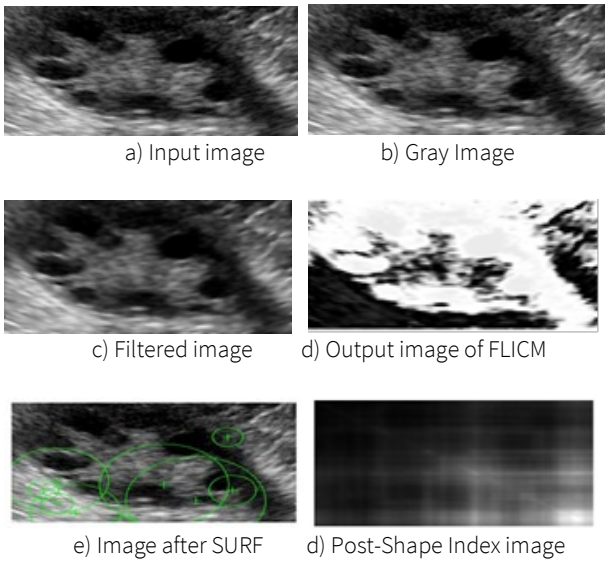

a) Input image b) Gray Image

c) Filtered image d) Output image of FLICM

e) Image after SURF d) Post-Shape Index image

Figure 3. Experimental outcomes of Ultrasound images a) input, b) Gray conversion, c) Filtered output d) FLICM output e) Image after SURF f|) Post-Shape Index image

4.4. Comparative techniques

To assess the adaptive AOA-DQN's performance for accurately identifying PCOS, it is compared to existing PCOS detection schemes, such as Thresholding method (Wisesty et al., 2018), Ensemble ML model with CNN (Suha & Islam, 2022), IFFOA-ANN (Nilofer & Ramkumar, 2021) and MLOD classifier (Kiruthika et al., 2020). The methods described above are tested using the same experimental settings and images from the Polycystic Ovary Ultrasound Images Dataset (Polycystic Ovary Ultrasound Images Dataset, 2023), and they are employed for a comparative valuation with different training data ang K-group values.

4.4.1. Assessment based on training data

The comparative discussion of proposed adaptive AOA-DQN based on training data is shown in Table 2. The comparative estimation of adaptive AOA-DQN for PCOS detection scheme is specified in figure 4. Here, the assessment is performed in terms of training data variations. The estimation regards to accuracy parameter is revealed in figure 4 a). For 60% of training data, accuracy of proposed adaptive AOA-DQN is 0.861, while the other techniques like Thresholding method, IFFOA-ANN, Ensemble ML model with CNN and MLOD classifier provided the accuracy of 0.811, 0.816, 0.827 and 0.830. Here the proposed adaptive AOA-DQN attained 5.757%, 5.205%, 3.935% and 3.632% of performance enhancement than other existing approaches. Likewise, the assessment in connection with sensitivity is revealed in figure 4 b). For 70% of training data, the sensitivity of AOA-DQN is 0.889, Thresholding method is 0.849, IFFOA-ANN is 0.861, Ensemble ML model with CNN is 0.869 and MLOD classifier is 0.865. Hence the proposed adaptive AOA-DQN has 4.482%, 3.225%, 2.286% and 2.780% of improved performance than others. Moreover, the assessment in terms of specificity is shown in figure 4 c). While 80% of training data, the specificity values like 0.864, 0.870, 0.888,0.888 and 0.906 are attained by the Thresholding method, IFFOA-ANN, Ensemble ML model with CNN, MLOD classifier and proposed adaptive AOA-DQN. Here, the proposed adaptive AOA-DQN provided 4.649%, 3.963%, 2.060% and 2.059% of better performance compared to others.

Table 2. Comparative discussion of proposed adaptive AOA-DQN based on training data.

Variations	Metrics / Methods Based on training data		
	Accuracy	Sensitivity	Specificity
Thresholding method	0.872	0.877	0.893
IFFOA-ANN	0.882	0.89	0.9
Ensemble ML model with CNN	0.882	0.888	0.904
MLOD classifier	0.879	0.879	0.907
proposed adaptive AOA-DQN	**0.906**	0.912	**0.928**

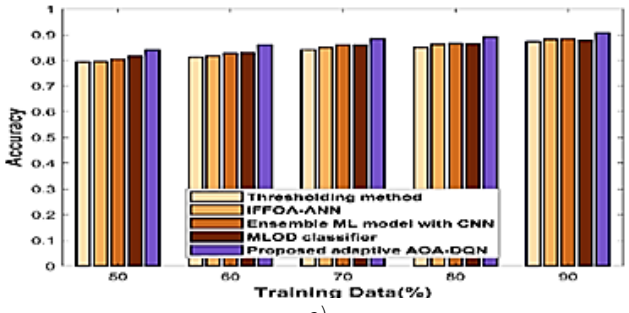

a)

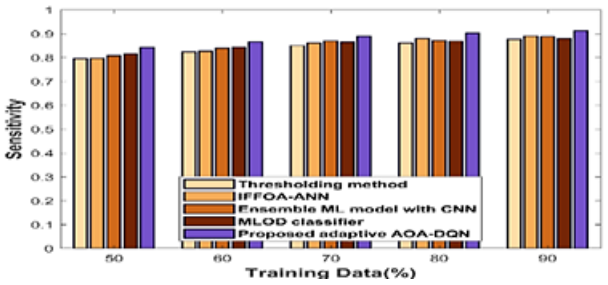

b)

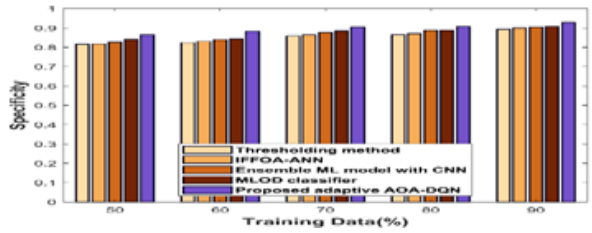

c)

Figure 4. Assessment of AOA-DQN using training data a) accuracy, b) sensitivity c) Specificity

4.4.2. Assessment based on K value

The comparative discussion of proposed adaptive AOA-DQN based on K value is shown in table 3. The comparative estimation of adaptive AOA-DQN with respect to K value variation is revealed in figure 5. The estimation regards to accuracy is presented in figure 5 a). For K value=8, accuracy of proposed adaptive AOA-DQN is 0.894, whereas the Thresholding method, IFFOA-ANN, Ensemble ML model with CNN and MLOD classifier attained the accuracy of 0.861, 0.863, 0.862 and 0.867. The proposed adaptive AOA-DQN achieved 3.654%, 3.440%, 3.542% and 2.917% of enhanced performance than other existing methods. Similarly, the evaluation in terms of sensitivity is deliberated in figure 5 b). For K value = 6, sensitivity of AOA-DQN is 0.883, Thresholding method is 0.816, IFFOA-ANN is 0.819, Ensemble ML model with CNN is 0.823 and MLOD classifier is 0.860. Here, the proposed adaptive AOA-DQN attained 7.535%, 7.286%, 6.723% and 2.570% of performance improvement compared to others. Furthermore, the analysis regards to specificity is revealed in figure 5 c). If the K value is 5, the specificity values of 0.806, 0.818, 0.833, 0.843 and 0.865 are provided by the Thresholding method, IFFOA-ANN, Ensemble ML model with CNN, MLOD classifier and proposed adaptive AOA-DQN. Hence, the proposed adaptive AOA-DQN achieved 6.783%, 5.475%, 3.657% and 2.564% of performance enhancement with respect to other existing techniques.

Table 3. Comparative discussion of proposed adaptive AOA-DQN based on K value.

Variations	Metrics / Methods Based on K value		
	Accuracy	Sensitivity	Specificity
Thresholding method	0.873	0.882	0.89
IFFOA-ANN	0.878	0.889	0.893
Ensemble ML model with CNN	0.882	0.892	0.897
MLOD classifier	0.885	0.899	0.898
Proposed adaptive AOA-DQN	0.904	**0.918**	0.917

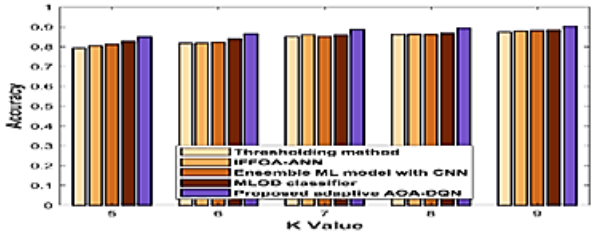

a)

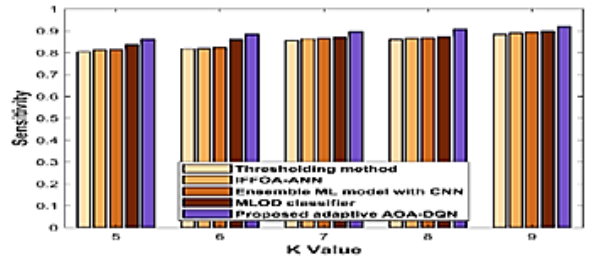

b)

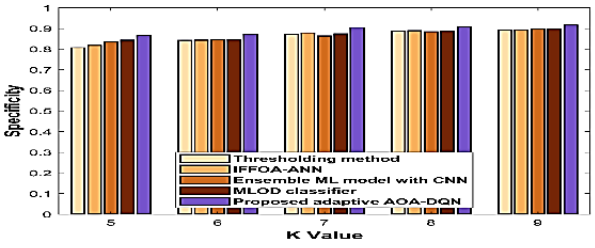

c)

Figure 5. Assessment of AOA-DQN using K-value a) accuracy, b) sensitivity c) Specificity.

4.5. Comparative discussion

The comparative discussion of the proposed adaptive AOA-DQN based on training data and K-values is shown in Figure 6. For training data variation, the proposed adaptive AOA-DQN attained the maximum value of accuracy is 0.906, while the Thresholding method, IFFOA-ANN, Ensemble ML model with CNN and MLOD classifier attained the accuracy is 0.872, 0.882, 0.882 and 0.879. The superior value of sensitivity 0.918 is attained by the proposed adaptive AOA-DQN in K fold value changes. Here, the sensitivity is 0.882 for the Thresholding method, 0.889 for IFFOA-ANN, 0.892 for the Ensemble ML model with CNN, and 0.899 for MLOD classifier. The maximum value of specificity 0.928 is attained by the adaptive AOA-DQN in terms of training data variation. Here, the specificity of other techniques like Thresholding method, IFFOA-ANN, Ensemble ML model with CNN and MLOD classifier is 0.893, 0.900, 0.904 and 0.907. The improved performance of the Adaptive AOA-DQN is due to optimized training through the Adaptive AOA algorithm, efficient learning via the Deep Q-Network (DQN), and comprehensive feature extraction, allowing more accurate classification compared to other methods.

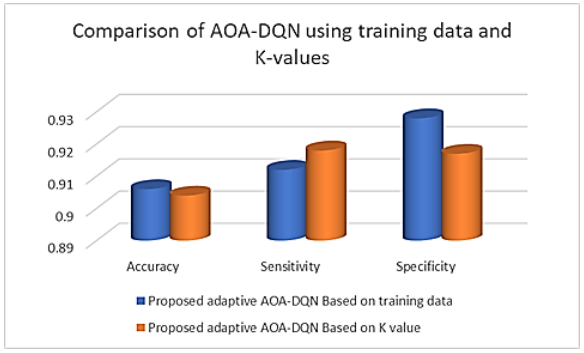

Figure 6. Comparison between AOA-DQN based on training data and K-value

5. Conclusions

PCOS is an endocrinological dysfunction that primarily affects the women of their reproductive age. PCOS is a group of syndromes characterized by a high level of androgens in women. This paper devised the optimized DL scheme for categorizing PCOS disease detection. In this work, the ultrasound input image is gathered from the dataset. To eliminate the noise from input image, the adaptive wiener filter is employed. The FLICM is utilized in PCO follicles segmentation process. The Feature extraction is considered as the next level of process, in which the SURF, Shape index histogram, and statistical features including variance, mean, kurtosis, entropy, and standard deviation are extracted. Moreover, the PCOS detection is performed in the following process with the help of adaptive AOA enabled DQN. Furthermore, the system performance is estimated using parameters such as accuracy, sensitivity, and specificity with the values like 0.906, 0.918 and 0.928 are attained. The enhanced performance can be attributed to several factors: efficient noise reduction through the Adaptive Wiener filter, accurate follicle segmentation with FLICM, thorough feature extraction including SURF, Shape Index Histograms, and statistical features, and the implementation of an Adaptive AOA-enabled DQN for optimized PCOS detection. In the future, different algorithms will be developed to progress the prediction process from all kinds of images.

Conflict of interest

The author has no conflict of interest to declare.

Funding

The author received no specific funding for this work.

References

Alamoudi, A., Khan, I. U., Aslam, N., Alqahtani, N., Alsaif, H. S., Al Dandan, O., ... & Al Bahrani, R. (2023). A deep learning fusion approach to diagnosis the polycystic ovary syndrome (PCOS). *Applied Computational Intelligence and Soft Computing*, *2023*(1), 9686697. https://doi.org/10.1155/2023/9686697

Bay, H., Ess, A., Tuytelaars, T., & Van Gool, L. (2008). Speeded-up robust features (SURF). *Computer vision and image understanding*, *110*(3), 346-359. https://doi.org/10.1016/j.cviu.2007.09.014

Deng, Y., Wang, Y., & Shen, Y. (2011). An automated diagnostic system of polycystic ovary syndrome based on object growing. *Artificial intelligence in medicine*, *51*(3), 199-209. https://doi.org/10.1016/j.artmed.2010.10.002

Gopalakrishnan, C., & Iyapparaja, M. (2020). Active contour with modified Otsu method for automatic detection of polycystic ovary syndrome from ultrasound image of ovary. *Multimedia Tools and Applications*, *79*(23), 17169-17192. https://doi.org/10.1007/s11042-019-07762-3

Gopalakrishnan, C., & Iyapparaja, M. (2019). Detection of polycystic ovary syndrome from ultrasound images using SIFT descriptors. *Bonfring International Journal of Software Engineering and Soft Computing*, *9*(2), 26-30.

Hashim, F. A., Hussain, K., Houssein, E. H., Mabrouk, M. S., & Al-Atabany, W. (2021). Archimedes optimization algorithm: a new metaheuristic algorithm for solving optimization problems. *Applied intelligence*, *51*(3), 1531-1551. https://doi.org/10.1007/s10489-020-01893-z

Hiremath, P. S., & Tegnoor, J. R. (2010a). Automatic detection of follicles in ultrasound images of ovaries using edge based method. *IJCA, Special Issue on RTIPPR*, *2*, 120-125.

Hiremath, P. S., & Tegnoor, J. R. (2010b). Follicle detection in ultrasound images of ovaries using active contours method. In *2010 International Conference on Signal and Image Processing* (pp. 286-291). IEEE. https://doi.org/10.1109/ICSIP.2010.5697484

Khairandish, M. O., Sharma, M., Jain, V., Chatterjee, J. M., & Jhanjhi, N. Z. (2022). A hybrid CNN-SVM threshold segmentation approach for tumor detection and classification of MRI brain images. *Irbm*, *43*(4), 290-299. https://doi.org/10.1016/j.irbm.2021.06.003

Kiruthika, V., Sathiya, S., & Ramya, M. M. (2020). Machine learning based ovarian detection in ultrasound images. *International Journal of Advanced Mechatronic Systems*, *8*(2-3), 75-85. https://doi.org/10.1504/IJAMECHS.2020.111306

Krinidis, S., & Chatzis, V. (2010). A robust fuzzy local information C-means clustering algorithm. *IEEE transactions on image processing*, *19*(5), 1328-1337. https://doi.org/10.1109/TIP.2010.2040763

Lawrence, M. J., Eramian, M. G., Pierson, R. A., & Neufeld, E. (2007). Computer assisted detection of polycystic ovary morphology in ultrasound images. In *Fourth Canadian Conference on Computer and Robot Vision (CRV'07)* (pp. 105-112). IEEE. https://doi.org/10.1109/CRV.2007.18

McLaughlin, M., Kelsey, T. W., Wallace, W. H. B., Anderson, R. A., & Telfer, E. E. (2017). Non-growing follicle density is increased following adriamycin, bleomycin, vinblastine and dacarbazine (ABVD) chemotherapy in the adult human ovary. *Human Reproduction*, *32*(1), 165-174. https://doi.org/10.1093/humrep/dew260

Nilofer, N. S., & Ramkumar, R. (2021). Follicles classification to detect polycystic ovary syndrome using GLCM and novel hybrid machine learning. *Turkish Journal of Computer and Mathematics Education*, *12*(7), 1062-1073.

Nasim, S., Almutairi, M. S., Munir, K., Raza, A., & Younas, F. (2022). A novel approach for polycystic ovary syndrome prediction using machine learning in bioinformatics. *IEEE Access*, *10*, 97610-97624. https://doi.org/10.1109/ACCESS.2022.3205587

Larsen, A. B. L., Vestergaard, J. S., & Larsen, R. (2014). HEp-2 cell classification using shape index histograms with donut-shaped spatial pooling. *IEEE transactions on medical imaging*, *33*(7), 1573-1580. https://doi.org/10.1109/TMI.2014.2318434

Polycystic Ovary Ultrasound Images Dataset. (2023). Polycystic Ovary Ultrasound Images Dataset. Accessed on February2023. https://dataverse.telkomuniversity.ac.id/dataset.xhtml?persistentId=doi:10.34820/FK2/QVCP6V

Sarty, G. E., Liang, W., Sonka, M., & Pierson, R. A. (1998). Semiautomated segmentation of ovarian follicular ultrasound images using a knowledge-based algorithm. *Ultrasound in medicine & biology*, *24*(1), 27-42. https://doi.org/10.1016/S0301-5629(97)00213-5

Sasaki, H., Horiuchi, T., & Kato, S. (2017). A study on vision-based mobile robot learning by deep Q-network. In *2017 56th Annual Conference of the Society of Instrument and Control Engineers of Japan (SICE)* (pp. 799-804). IEEE. https://doi.org/10.23919/SICE.2017.8105597

Suha, S. A., & Islam, M. N. (2022). An extended machine learning technique for polycystic ovary syndrome detection using ovary ultrasound image. *Scientific Reports*, *12*(1), 17123. https://doi.org/10.1038/s41598-022-21724-0

Shabani, S., Samadianfard, S., Sattari, M. T., Mosavi, A., Shamshirband, S., Kmet, T., & Várkonyi-Kóczy, A. R. (2020). Modeling pan evaporation using Gaussian process regression K-nearest neighbors random forest and support vector machines; comparative analysis. *Atmosphere*, *11*(1), 66. https://doi.org/10.3390/atmos11010066

Viher, B., Dobnikar, A., & Zazula, D. (1998). Cellular automata and follicle recognition problem and possibilities of using cellular automata for image recognition purposes. *International journal of medical informatics*, *49*(2), 231-241. https://doi.org/10.1016/S1386-5056(98)00042-2

Wisesty, U.N., Nasri, J., Adiwijaya (2017). Modified Backpropagation Algorithm for Polycystic Ovary Syndrome Detection Based on Ultrasound Images. In: Herawan, T., Ghazali, R., Nawi, N.M., Deris, M.M. (eds) Recent Advances on Soft Computing and Data Mining. (SCDM 2016). Advances in Intelligent Systems and Computing, vol 549. Springer, Cham. https://doi.org/10.1007/978-3-319-51281-5_15

Wisesty, U. N., Thufailah, I. F., Dewi, R. M., Adiwijaya, & Jondri, (2018). Study of Segmentation Technique and Stereology to Detect PCO Follicles on USG Images. *Journal of Computer Science*, *14*(3), 351-359. https://doi.org/10.3844/jcssp.2018.351.359

Wu, F., Yang, W., Xiao, L., & Zhu, J. (2020). Adaptive wiener filter and natural noise to eliminate adversarial perturbation. *Electronics*, *9*(10), 1634. https://doi.org/10.3390/electronics9101634